Petroleum Science 19 (2022) 100–115

Contents lists available at ScienceDirect

Petroleum Science

journal homepage: www.keaipublishing.com/en/journals/petroleum-science

Original Paper

Influence of structural damage on evaluation of microscopic pore structure in marine continental transitional shale of the Southern North China Basin: A method based on the low-temperature N_2 adsorption experiment

Mei-Ling Han [a], Xiao-Liang Wei [b], Jin-Chuan Zhang [a, *], Yang Liu [a], Xuan Tang [a], Pei Li [c], Zi-Yi Liu [d]

[a] Key Laboratory of Strategy Evaluation for Shale Gas of Ministry of Land and Resources, China University of Geosciences, Beijing, 100083, China
[b] Exploration and Development Institute of Shengli Oilfield Company, Sinopec, Dongying, Shandong 257015, China
[c] Petroleum Exploration and Production Research Institute, China Petroleum and Chemical Corporation (Sinopec), No. 197 Baisha Road, Changping District, Beijing, 102206, China
[d] State Key Laboratory of Petroleum Resources and Prospecting, China University of Petroleum, Beijing, 102200, China

ARTICLE INFO

Article history:
Received 4 January 2021
Accepted 15 July 2021
Available online 25 October 2021

Edited by Jie Hao

Keywords:
Marine continental transitional shale
N_2 adsorption
Structural damage
Crushing mesh
Pore structure parameters

ABSTRACT

Structural damage from sample preparation processes such as cutting and polishing may change the pore structure of rocks. However, changes in pore structure caused by this structural damage from crushing and its effect on marine continental transitional shale have not been well documented. The changes of microscopic pore structure in marine continental transitional shale during the sample preparation have important research value for subsequent exploration and development of shale gas. In this study, the pore structures of transitional shale samples from the Shanxi-Taiyuan Formation of the Southern North China Basin under different degrees of damage were analyzed through low-temperature N_2 adsorption experiments, combined with X-ray diffraction, total organic carbon, vitrinite reflectance analysis, and scanning electron microscopy. The results showed that (1) With increasing structural damage, the specific surface area (SSA) changed within relatively tight bounds, while the pore volume (PV) varied significantly, and the growth rate (maximum) exhibited a certain critical value with the crushing mesh number increasing from 20 to 200. (2) The ratio of SSA to PV can be used as a potential proxy for evaluating the influence of changes in the pore structure. (3) Correlation analysis revealed that the microscopic pore structure of marine continental transitional shale from the Shanxi-Taiyuan Formations is mainly controlled by organic matter and clay minerals. Clay minerals play a leading role in the development of microscopic pores and changes in pore structure.

1. Introduction

With the successful development of shale gas in North America and the optimization of the global energy structure, oil-gas resources in shale reservoirs have gradually become the focus of exploration and development in many countries (Desbois et al., 2011; Zou et al., 2012; Wang et al., 2017). Marine continental transitional facies are important characteristics of shale gas in China and have broad prospects for shale gas resources (Li et al., 2019). The Southern North China Basin is an important place for the distribution of marine continental transitional shale in China. The transitional organic-rich black shale of Taiyuan-Shanxi Formation widely developed in the basin has typical characteristics of stable deposition, large accumulated thickness and high gas content, which is of great research value. At present, successful achievements have been made in the exploration and development of shale gas in marine shale. However, the transitional shale of China, which also has good resource potential, has not been extensively studied, thus hindering breakthroughs (Yang et al., 2017; Li et al., 2019).

* Corresponding author.
E-mail address: zhangjc@cugb.edu.cn (J.-C. Zhang).

https://doi.org/10.1016/j.petsci.2021.10.016

Tight shale reservoirs are essentially a porous medium, and their spatial structure is composed of pores and a solid matrix (Ambrose et al., 2012; Loucks et al., 2012; Gu et al., 2015). Nano-micron pores are the main enrichment space for oil and gas in tight reservoirs (Ross and Bustin, 2009; Zhang et al., 2012; Gao and Li, 2016). Therefore, the study of microscopic pore structure has important theoretical significance for revealing the pore development characteristics as well as the gas-storage performance (Tong et al., 2017). Previous studies have shown that the transitional shale in China is mainly developed in the coal-bearing strata of the Carboniferous-Permian, often interbedded with coal and tight sandstone. Transitional shale has a much higher clay mineral content than marine or continental shale. The degree of evolution of organic matter is generally at the stage of maturity to overmaturity, with strong heterogeneity. In contrast to marine or continental shale, the pore types of transitional shale are mainly clay mineral pores, with relatively poor development of organic-matter pores. The pores are mostly narrow slits of granular inner pores and mineral intergranular pores (Tang et al., 2016; Li et al., 2019). Based on this feature, gas adsorption (including nitrogen, argon, and carbon dioxide) has become the main method for evaluating pore structure at present. In recent years, considering the simplicity of operation and economic practicability, most scholars have selected N_2 adsorption experiments (Han et al., 2016; Mastalerz et al., 2017; Zhang et al., 2017) in combination with the statistical analysis of particular parameters, such as the specific surface area (SSA), pore volume (PV), and pore size distribution (PSD) to study the microscopic pore characteristics.

Previous studies have shown that particle size has a certain influence on the experimental results of microscopic pores in tight reservoirs (Desbois et al., 2011; Slatt and O'Brien, 2011; Pommer and Milliken, 2015; Mastalerz et al., 2017). During sample preparation, particle size is often changed through grinding and crushing. At the micro level, the structure and internal composition of tight reservoirs will inevitably change, damaging the pore structure (Lee, 2012; Boudriche et al., 2014). Therefore, differences in particle size are essentially a reflection of different degrees of structural damage. Structural damage from sample preparation has a certain influence on the qualitative and quantitative evaluation of micropores in tight shale reservoirs. In recent years, scholars have focused on this problem in tight reservoirs, particularly in tight sandstone, coal, and marine shale. Y. Li et al. (2019) explored the effects of different particle sizes on the experimental results of low-temperature N_2 adsorption of Gaotaizi tight sandstone in the Songliao Basin. The results showed that the pore parameters (PV and SSA) varied according to different particle sizes. In coal, changes in particle size affect methane adsorption mainly by changing the SSA and pore structure (Bertard et al., 1970; Nandi et al., 1975; Busch et al., 2004). In a study of Devonian Mississippian New Albany shale samples, Wei et al. (2014) and Chen et al. (2015a,b) found that particle size could affect gas adsorption experimental data. However, potential changes in the pore-fracture system induced by structural damage and their influence on microscopic pore structure evaluation of marine continental transitional shale have rarely been studied. This study explored the specific impact of structural damage on the microscopic pore system of transitional shale during sample preparation through the statistics and analysis of experimental data on nitrogen adsorption using core samples from the Shanxi Formation and Taiyuan Formation in the Southern North China Basin. The main objectives of this study are as follows: (1) Comprehensively analyze the variation characteristics of micropores and mesopores in transitional shales with different degrees of structural damage; (2) Summarize the error effect of damage from sample preparation on the nanoscale pore structure, which would provide effective and reasonable reference information for the qualitative and quantitative evaluation of pore structure and gas-storage capacity of shale; (3) Describe the main factors controlling the development of transitional shale pores under different degrees of structural damage.

2. Geological setting

The Southern North China Basin, located in the south of the North China platform, is a meso-Cenozoic superimposed basin developed on the North China platform (Jiang, 2016). The South China North Basin consists of five structural units, from north to south: Kaifeng Depression, Taikang Uplift, Zhoukou Depression, Bengbu Uplift, and Xinyang-Hefei Depression (Fig. 1a and b). The Permian strata in the basin are mainly distributed in the Kaifeng Depression, Zhoukou Depression, and Taikang Uplift, with a thickness of over 100 m. From the Late Ordovician to the Middle Carboniferous, the North China Plate was gradually uplifted by the Caledonian movement. A long period of weathering and denudation caused widespread loss of the upper Ordovician-early Carboniferous strata in this area. Therefore, the transitional facies strata of the Permian in the Southern North China Basin were directly deposited on the Ordovician limestone. The sedimentary environment during this period was changeable and was mainly controlled by regional tectonic movements. In the early Carboniferous, the North China platform re-sank, and seawater invaded from northeast to southwest, forming a widely distributed North China surface sea. Until the early Permian, the Taiyuan Formation was composed of shale, coal, and siltstone, with a thickness ranging from 30 m to 175 m. Subsequently, due to the collision between the North China Plate and the Siberian Plate, the North China Plate was uplifted again, and seawater receded from north to south. In this process, the Southern North China Basin formed a complex sedimentary system dominated by shallow coastal seas and river deltas. The Shanxi Formation is composed of shale, coal, siltstone, and sandstone, and its thickness ranges from 50 m to 130 m (Jiang, 2016; Dang et al., 2018).

Well Zhengxiye-1 is located in the Wenxian block of Henan Province. Its structural location is in the transitional zone between the southern Taikang Uplift and the northern Kaifeng Depression (Dang et al., 2018). Well Zhengxiye-1 contains the gas-bearing interval of Taiyuan and Shanxi Formations about 130 m behind, with the well depth ranging from 3250 to 3379 m. The Shanxi Formation and Taiyuan Formation strata selected for the target interval are a set of typical marine continental transitional facies deposits with depths ranging from 3260 m to 3345 m and a thickness of 85 m. The lithology of the Taiyuan Formation is black, gray-black mudstone, black silty mudstone, and limestone, which are mixed with coal lines. The lithology of the Shanxi Formation is mainly black, gray-black mudstone, silty mudstone, fine sandstone, and sandstone, which contain a large amount of carbon debris. The five shale samples selected in this study are from the high-quality transitional gray-black shale section of the Taiyuan Formation and Shanxi Formation. The limestone sample is from the thick-limestone section of the Taiyuan Formation.

3. Samples and analytical methods

3.1. Sample preparation

In this study, six core samples of the Shanxi and Taiyuan Formations from Well Zhengxiye-1 were selected as the research targets, consisting of five shale samples (JX-6, JX-13, JX-25, JX-44, JX-52) and a limestone sample (JX-46) (Fig. 1c). The six samples were collected from a depth interval ranging from 3265 m to 3345 m.

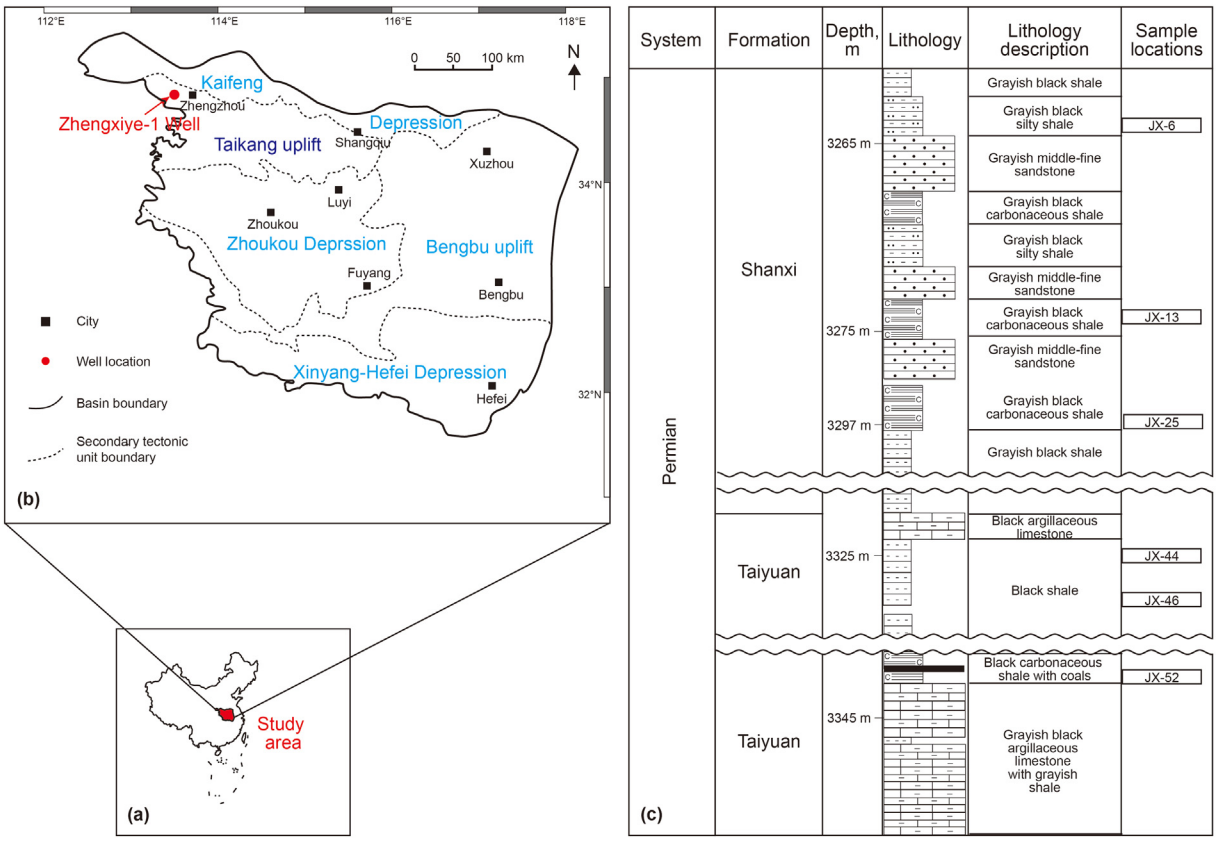

Fig. 1. (a) Location of Southern North Basin in China; (b) Tectonic unit division of Southern North Basin; (c) Stratigraphic columns of target interval.

To ensure the rationality of comparing experimental data, the six samples were first crushed and 20 mesh particles were screened out. Subsequently, the screened 20 mesh samples were divided into three parts; 2/3 of the 20 mesh particles were crushed to 80 mesh and 200 mesh, respectively. After the nitrogen adsorption experiment, the 200 mesh samples were analyzed for total organic carbon (TOC) content analysis, X-ray diffraction (XRD) for quantitative analysis of whole rock minerals and clay minerals, vitrinite reflectance analysis (R_o), and scanning electron microscopy (SEM) (Fig. 2).

3.2. Analytical methods

3.2.1. Organic petrography and mineralogical analysis

The TOC content of the samples was analyzed using a CS-230 Carbon and Sulfur elemental analyzer (LECO Corporation, USA) at the Sichuan Keyuan Engineering Technology Testing Center. The main pretreatment process of the samples can be described as follows: (1) Selection of powder samples after N_2 adsorption experiment; (2) Inorganic carbon removal using a certain concentration of hydrochloric acid solution (the ratio of pure hydrochloric acid to water is 1:7), and (3) Washing the residual acid, and placing the samples in an oven at 70–80 °C for drying. Sample preparation and measurements followed the standards of the International Union of Pure and Applied Chemistry (ICCP 1975; Strapoc et al., 2010; Wei et al., 2014; ASTM 2016).

Vitrinite reflectance R_o (%) measurements were performed using an MPV-SP microscope and a 308-PV microscope photometer. The processing procedure of the test samples was as follows: (1) grinding and polishing the samples into specific light sheets and drying the light sheets; (2) using a microphotometer to calibrate the standard sample by the double standard method; and (3) data processing.

Pore morphology was observed using a Zeiss EVO-15 scanning electron microscope with a smart energy-dispersive spectrometer (Zeiss SmartEDS). Six samples polished with an argon ion beam were scanned at an accelerated voltage ranging from 0.2 to 30 kV, and the surface of the transitional shale samples was coated with a layer of Au (99.999% purity) (Li et al., 2019). Argon ion polishing can create a smooth plane for observing the morphological characteristics of pores, and Zeiss SmartEDS was used for elemental analysis (Shi et al., 2015).

XRD measurements of the powder samples were performed using a Bruker D8 DISCOVER diffractometer (CuKα radiation). A scan rate of 4°(2θ)/min was used in the range of 5–45° to record the XRD traces. Minerals were identified using Bruker DiffracPLUS EVA software, and then quantitatively analyzed using Rietveld refinement in the Bruker DiffracPLUS TOPAS software (Xiong et al., 2017). Non-clay mineral content was measured using the K-value method after Rietveld refinement (Rietveld and MacKay, 1969), and the contents of various clay minerals were calculated using a suspension separation method. The experiment was also completed at the Sichuan Keyuan Engineering Technology Testing Center.

3.2.2. N_2 adsorption analysis and data processing

The low-temperature nitrogen adsorption experiment was carried out at the China University of Geosciences (CUGB), using an Autosorb-iQ specific surface area and pore size analyzer (Quantachrome Instruments). Six core samples from Well Zhengxiye-1 were ground to 20, 80, and 200 mesh to determine the nitrogen adsorption capacity under different equilibrium pressures. The specific experimental steps are as follows: (1) Vacuum degassing.

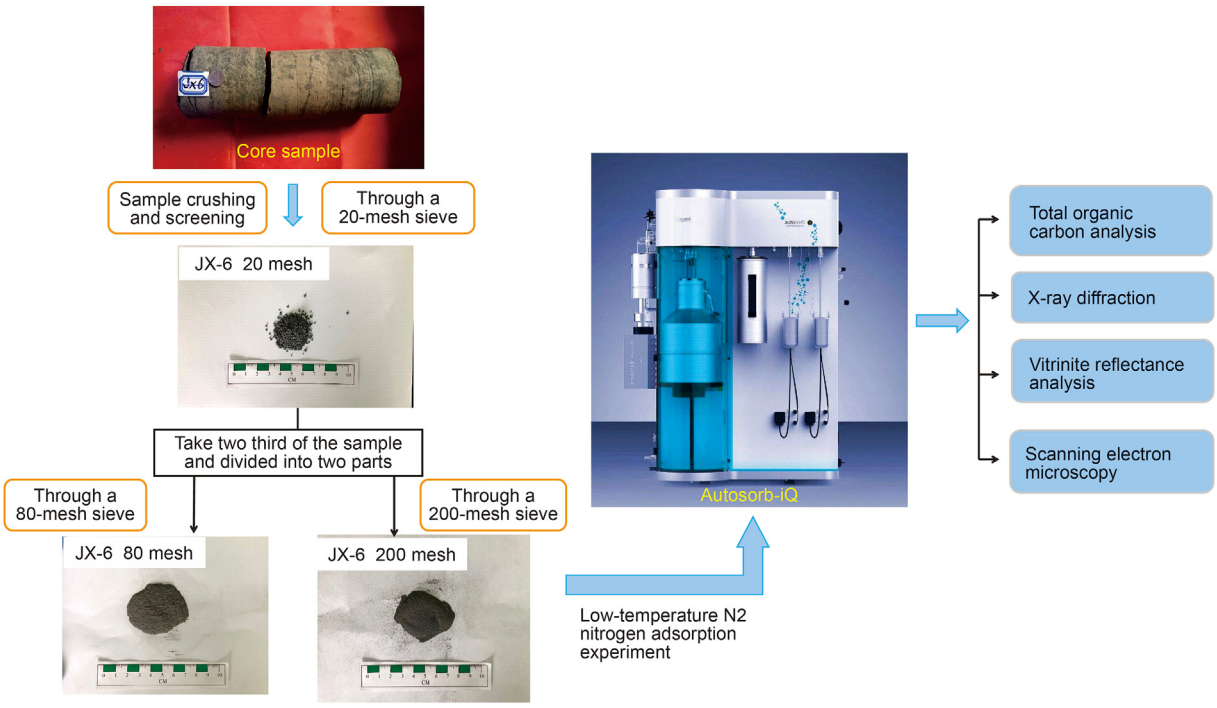

Fig. 2. Sample processing diagram (Take JX-6 as an example).

All samples were degassed under vacuum for 9 h at a temperature of 90 °C; (2) Sample weighing. The difference between the mass of the sample tube after degassing and the mass of the empty tube before degassing is the mass of the sample after vacuum degassing; (3) Cooling and measurement. The experimental samples were cooled in liquid nitrogen at the temperature of liquid nitrogen (77.35 K, −196 °C), the amount of nitrogen adsorbed at multiple preset pressure points was measured, and the adsorption-desorption isotherms of six samples under different mesh numbers were obtained.

Common macroscopic thermodynamic methods for analyzing the microscopic pore structure of porous media based on gas adsorption include the Langmuir monolayer adsorption theory, multilayer adsorption theory (leading to the Brunauer-Emmet-Teller (BET) equation) (Jaroniec, 1983; Rundzinski and Ecerett 1992), capillary condensation theory based on the Kelvin equation (such as the Barrett-Joyner-Halenda (BJH) method), and Dubinin-Polanyi adsorption potential theory (such as the Dubinin—Astakhov (DA) equation) (Artur et al., 2002). Relative to these macroscopic methods, the density functional theory (DFT) and Monte Carlo method (MC) are based on molecular dynamics. The non-local density functional theory (NLDFT) and MC provide more accurate fluid structures in narrow pores; they not only provide a microscopic model of adsorption but also more realistically reflect the thermodynamic properties of fluids in pores (Yang and Martias, 2009).

Recent researches have shown that NLDFT is a superior alternative to computational theories based on physical models for the analysis of micropores and mesopores in porous media (Landers et al., 2013). Compared differences between model analyses, data points in the range of P/P_0 (from 0.01 to 0.995) were selected in this study, and the NLDFT model was used to calculate the PV of the micropores. The BJH model were used to calculate the PV and pore size distribution (PSD) of the mesopores. According to the adsorption isotherm data, data points with a relative pressure between 0.05 and 0.35, were selected, and the BET equation was used to calculate the SSA of the samples.

4. Results

4.1. Organic geochemistry and mineral composition

The formation, R_o, TOC content, and mineral composition of the samples are presented in Table 1. The six samples had high vitrinite reflectivity (R_o) ranging from 4.16% to 4.47%. Limestone sample JX-46 contained no clay minerals, and the TOC content of the other samples ranged from 0.7% to 2%, with an average of 1.04%. The vitrinite reflectance R_o of all the shale samples were above 4.0, indicating they were in the over-maturity stage during the thermal evolution of organic matter.

The results of XRD mineral composition analysis of the samples showed that the main mineral components are quartz and clay minerals, accounting for approximately 80%–90% of the relative content of the main minerals. Except for the limestone sample JX-46, the quartz content of the other shale samples was between 27% and 45% (with an average of 34.8%), while clay minerals accounted for approximately 31%–63% of the total mineral composition (with an average of 52.4%). Illite was the most commonly developed clay mineral with the highest content in the studied interval, followed by illite-smectite mixed clay (I/S), which accounted for approximately 70%–90% of clay minerals. In addition, these samples also contained a small amount of kaolinite and chlorite. The combination characteristics of clay minerals suggest that the Shanxi and Taiyuan Formations in the study area have undergone the late diagenesis stage.

4.2. Low-temperature N_2 adsorption

4.2.1. Isotherms

The isotherms of the six samples with different particle sizes treated under the same experimental conditions are shown in Fig. 3. The isotherm of JX-46 limestone sample represents the Type III, and there is no inflection point “B” which is the symbol of the end of the single-layer adsorption. When the relative pressure ($P/$

Table 1
Total organic carbon (TOC) content, equivalent vitrinite reflectance (R_o) and mineral composition of samples.

Samples	*Ro* (%)	TOC (wt., %)	Mineral composition (wt, %)						Clay mineral composition (wt, %)			
			Quartz	Feldspar	Calcite	Dolomite	Pyrite	Clay	Kaolinite	Chlorite	Illite	I/S
JX-6	4.47	1.246	32	5	–	–	–	63	–	3	79	18
JX-13	4.22	0.5228	27	10	–	–	–	63	15	4	55	26
JX-25	4.16	0.7	42	3	3	10	–	42	5	26	61	8
JX-44	4.18	1.982	28	5	–	–	4	63	4	14	70	12
JX-46	4.16	0.3368	7	–	93	–	–	–	–	–	–	–
JX-52	4.27	0.7433	45	3	–	8	1	31	13	6	71	10

Note: "–" indicates that the mineral component in the sample has not been detected.

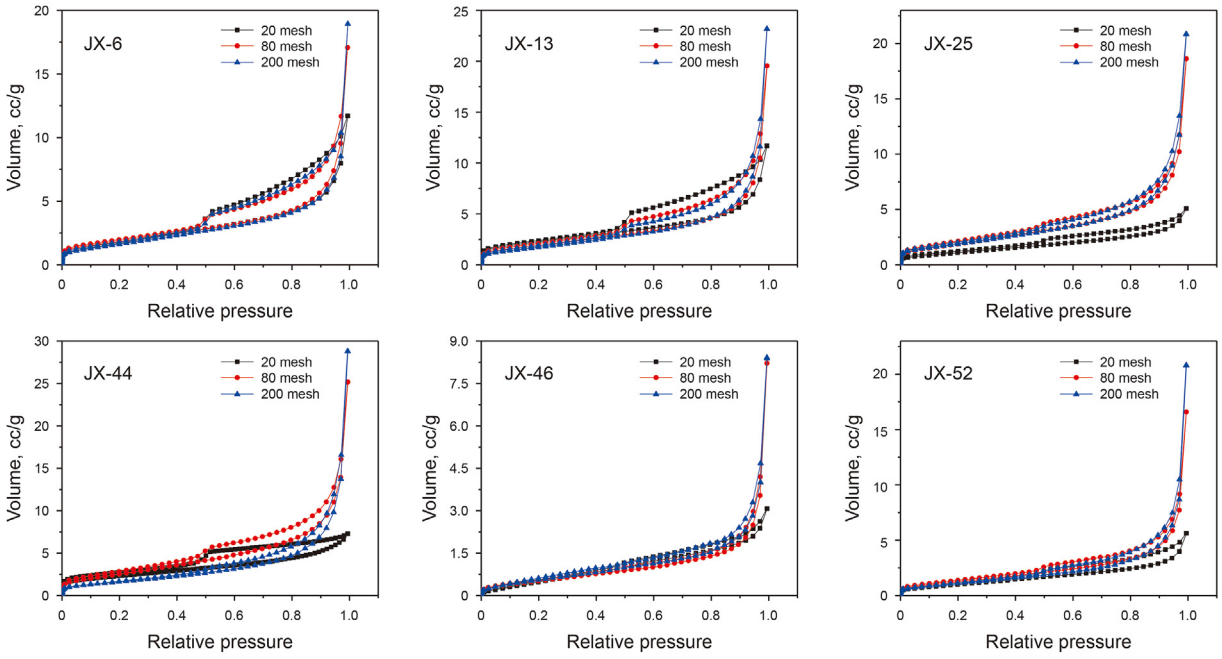

Fig. 3. Line graphs of low-temperature N_2 adsorption isotherms of six samples.

P_0) is close to 1, the isotherm has no platform, indicating that this type of adsorption isotherm is mainly formed by microporous materials. In fact, the JX-46 limestone sample is mainly composed of calcite and quartz. The internal pores are dominated by larger dissolved pores, and the force between the material and the adsorbed gas is really weak. The adsorption isotherm of JX-6, 13, 25, 44, 52 shale samples represent the Type IV, which indicates that multi-layer adsorption has occurred in the studied samples, accompanied by a capillary condensation process (Thommes et al., 2015). These isotherms are characterized by obvious hysteresis at the relative pressure P/P_0 between 0.4 and 0.5, indicating that the adsorption and desorption branches do not coincide, which represents the isotherm of the materials with larger mesopores.

The shape of these isotherms exhibited an inverse "S" type. In the low-pressure section ($P/P_0 < 0.1$), the adsorption isotherm is inclined to the Y-axis, indicating that there is a certain amount of micropores and a strong interaction between the materials and nitrogen. The strong adsorption potential of micropores makes the pore surface appear a single molecular layer of adsorption. In the medium-pressure section ($0.1 < P/P_0 < 0.9$), it is the condensation accumulation of nitrogen in the pores. The adsorption capacity increased slowly with increasing relative pressure, and the isotherms were approximately linear, indicating that with the continuous increase of gas molecules, due to the large number of mesopores in the sample, the adsorption of nitrogen on the pore surface is a multi-molecular layer. In the high-pressure section ($0.9 < P/P_0 < 1.0$), the isotherms rose rapidly. When the relative pressure P/P_0 was close to 1, the adsorption isotherms did not show a platform (adsorption saturation phenomenon). This indicates that the gas is mainly adsorbed on the larger pores (mesopores or macropores), and the increase of the proportion of larger pores provides more adsorption space for nitrogen, and the gas adsorption capacity increases significantly.

4.2.2. Surface area and pore volume

The SSA and PV data obtained from the low-temperature N_2 adsorption experiment with the crushing mesh number from 20 mesh to 80 mesh–200 mesh are shown in Table 2. The BET model was used to calculate SSA, and the BJH and NLDFT models were used to calculate PV.

The results of N_2 adsorption experiments showed that the SSA values varied with the mesh increasing from 20 to 80 to 200, but the overall SSA showed only slight variations, ranging from 0.1% to 70% (Fig. 4a). The PV values also varied, with a significant overall variation, increasing from 1% to 300% (Fig. 4b). As the crushing mesh was increased, the PV value showed varying degrees of change. During the crushing process from 20 to 80 mesh, the particle size decreased from 850 μm to 180 μm, PV became larger, and the total PV of the pores increased significantly. From 80 to 200 mesh, the particle size decreased from 180 μm to 75 μm and PV continued to increase, but the growth rate of PV was significantly reduced compared with that of the 20–80 mesh crushing.

Table 2
SSA and PV values of samples under different crushing meshes.

Samples	SSA, m^2/g					PV, cc/g				
	20 mesh	80 mesh	200 mesh	20-80 growth rate, %	80-200 growth rate, %	20 mesh	80 mesh	200 mesh	20-80 growth rate, %	80-200 growth rate, %
JX-6	6.897	6.778	6.471	−1.73	−4.53	0.0181	0.0264	0.02155	45.86	−18.37
JX-13	8.168	7.223	6.748	−11.57	−6.58	0.0181	0.03023	0.03585	67.29	18.59
JX-25	4.414	7.384	7.212	67.29	−2.33	0.0079	0.02882	0.03226	265.09	11.94
JX-44	8.18	9.993	6.185	22.16	−38.11	0.0113	0.03895	0.04453	244.69	14.33
JX-46	2.703	2.186	2.387	−19.13	9.19	0.0048	0.01271	0.01296	167.47	1.97
JX-52	4.09	4.99	4.413	22.00	−11.56	0.0087	0.02567	0.03217	194.89	25.32

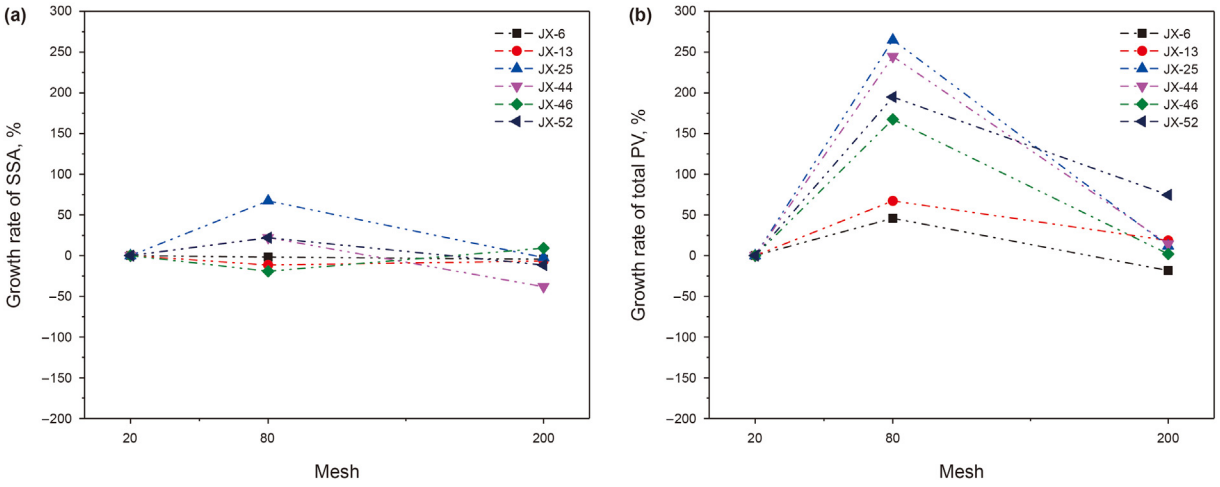

Fig. 4. The growth rate of SSA (a) and total PV (b) with different crushing meshes.

Moreover, the total PV increased, but the growth rate was lower than that of the 20–80 mesh crushing.

In the process of increasing the mesh number from 20 mesh, 80 mesh–200 mesh, the structural characterization parameters of micropores and mesopores showed different rules, and PV values exhibited various changes with the increasing mesh (Fig. 5). The PV value of micropores showed little change with increasing meshes, while those of mesopores and macropores significantly varied. In the process of grinding the samples from 20 to 80 mesh, the growth rate of PV showed a trend of significant increase. In the process of grinding the samples from 80 to 200 mesh, the growth rate of PV decreased significantly or no longer increased.

4.2.3. Pore size distribution

The pore size distribution (PSD) of each sample obtained using the BJH calculation model with the crushing mesh number is shown in Fig. 6. In this study, as the samples contained a large amount of micropores and mesopores, the PSD calculated can be expressed by the curve of differential pore volume ($dV/d(d)$) to pore size (Tian et al., 2013). The curve of the differential pore volume to pore size represents the change rate of pore volume with pore size. The graph area bounded by the aperture distribution curve and coordinate axis represents the PV.

The PSD diagrams for different pore types show that the PSD curve generally presents a single-peak feature, and all the peaks corresponding to particle size were below 10 nm. The pores larger than 10 nm of the JX-6, 13, 25, 44 and 52 shale samples were increased with the mesh number raising from 20 to 80 and 200. When the mesh number increases from 20 to 80, the pores at 2–50 nm of the JX-46 limestone sample increased greatly. In addition, when the mesh number of the limestone sample was increased from 80 to 200, the pores at 2–50 nm of the JX-46

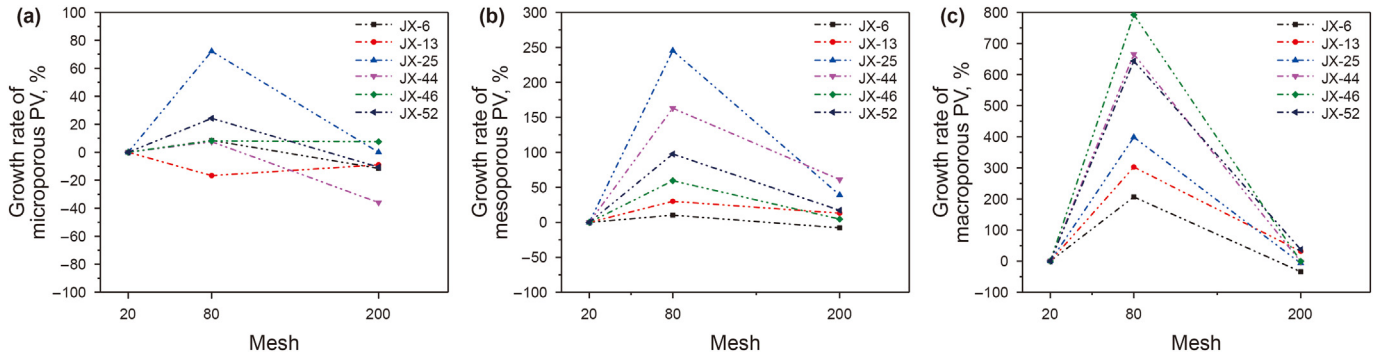

Fig. 5. The growth rate of PV in micropores (a), mesopores (b), macropores (c).

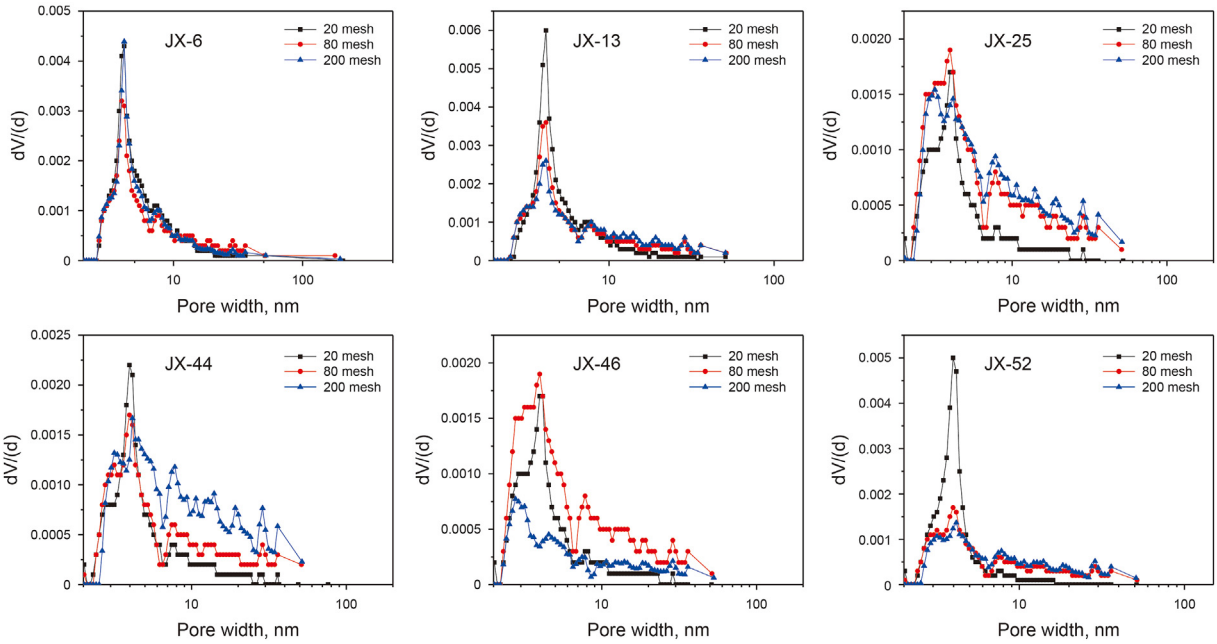

Fig. 6. The pore size distribution of micro-pores.

limestone sample decreased greatly. In general, whether the number of pulverized mesh is 20 mesh, 80 mesh or 200 mesh, for particle sizes of 3–10 nm, the peak of samples reached the maximum, which shows that the change rate of PV with pore size is the largest and there are mainly micropores and mesopores (pore size range: 2–50 nm) in the studied samples. Therefore, it can be found that different crushing meshes have a certain influence on the pore structure, and with the increase of crushing mesh number, the volume of mesopores and macropores is significantly increased due to the newly formed secondary pores.

5. Discussion

5.1. Morphology characteristics of transitional shale pores

5.1.1. Gas adsorption hysteresis loops

The shape of hysteresis can also indicate the characteristics of microscopic pores in different shale samples (Fig. 7). According to the International Union of Pure and Applied Chemistry (IUPAC), hysteresis loops are divided into four types: The Type H1 loop is narrow and is often found in materials that have a narrow range of cylindrical mesopores. Hysteresis loops of Type H2 have a very steep desorption branch, with a sharply decreasing inflection point. It often occurs in mesoporous materials with a narrow range of pore necks and a wide-body or "ink bottle" pores. The Type H2(a) usually represents "ink bottle" shaped pores with a thin pore neck and wide-body, while H2(b) represents the "ink bottle" shaped pores with a much larger neck width. Isotherms of the Type H3 loop rise rapidly with increasing relative pressure, and no adsorption saturation occurs when the relative pressure is close to 1. It often appears in mesoporous materials with a layered structure aggregation and wedge-shaped pores. With increasing relative pressure, the adsorption-desorption isotherms of Type H4 rise slowly, and adsorption saturation occurs when it is close to the saturated vapor pressure. This type usually occurs in materials with both micropores and mesopores. Hysteresis loops of Type H5 are unusual, and they have been found in mesoporous materials with partially blocked channels (Thommes et al., 2015; Zhang, 2017).

The shapes of the isotherms indicate the occurrence of three types of pores in the shale (Fig. 3). The adsorption isotherms of the low-pressure section exhibited a small change, while the isotherms of the high-pressure section exhibited a steep increase, and the gas adsorption capacity increased rapidly. Previously described experimental data have shown that with increasing mesh number, the SSA changed slightly, the proportion of micropores in the samples was generally maintained, and the large increase in nitrogen adsorption capacity in the high-pressure section was related to the content of larger pores. The increase of the proportion of larger pores (mainly mesopores and macropores) in the pore system provides more adsorption space for nitrogen. In addition, compared with the other five shale samples, the gas adsorption capacity of JX-46 was the lowest, The JX-46 limestone sample is mainly composed of calcite and quartz. The internal pores are dominated by larger dissolved pores (Fig. 3), which indicates that the internal pores of clay minerals and organic matter provide the main storage space for gas adsorption.

In fact, the internal structure of the shale micropore system is very complex and diverse. The shape of the adsorption-desorption isotherms is often a combination of multiple types. The shapes of the hysteresis loops of the samples exhibited various shapes according to different meshes (Fig. 3). When the crushing mesh was 20, the hysteresis loop of the studied samples mainly corresponded to Type H4, with mainly parallel slit-shaped pores. When the crushing mesh was 80 and 200, the hysteresis loop of the samples mainly corresponded to Type H3, indicating the dominance of wedge-shaped pores. Considering that the content of clay minerals in marine continental transitional shale is very high, the pore fractures between clay minerals are usually wedge-shaped and parallel slit-shaped (Milner et al., 2010; Kuila and Prasad, 2013; Yang et al., 2016). Therefore, the flat hysteresis loops of marine continental transitional shale are believed to be attributable to the pores in clay minerals. The interlayer pores of the clay minerals were dominant in the pore-fracture system of the transitional shale. The content of developed pores (organic-matter (OM) pores) was low, which also explains the poor development of OM pores in the transitional facies shale.

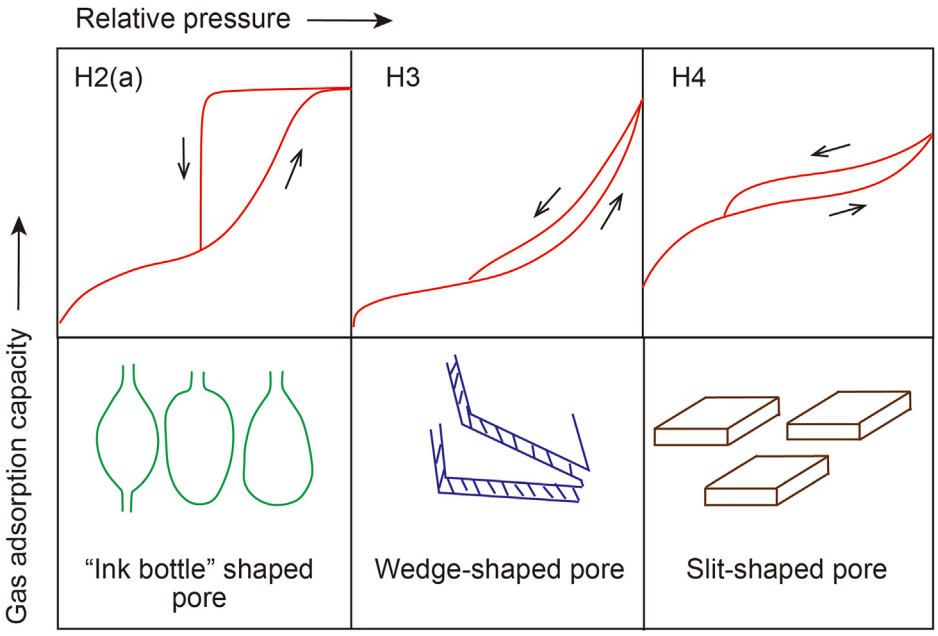

Fig. 7. Schematic diagram of typical hysteresis loop types and corresponding pore morphology (Modified from IUPAC, 2015)

Furthermore, the difference in the shape of the hysteresis loops with crushing meshes is attributable to the pore characteristics of different types of clay minerals. The transitional shale clay minerals of the Shanxi and Taiyuan Formations are mainly illite and the illite-smectite mixed clay (I/S). By virtue of its structure, I/S has an inner surface and an outer surface, and its internal pores can form parallel slit-shaped pores. Illite can only produce wedge-shaped pores formed by the loose accumulation of single flake crystals. Therefore, for shale samples with high illite content, the shape of the hysteresis loop is mostly Type H3; for shale samples with a high I/S content, the shape of the hysteresis loop is mostly Type H4. The above experimental results indicate that with increasing crushing mesh from 20 to 80–200 mesh, the hysteresis loops of the samples changed from Type H4 to Type H3; in other words, with increasing degree of structural damage, the proportion of I/S decreased and that of illite increased. At the same time, it also proves that increases in the degree of damage affect the pore structure of I/S.

5.1.2. Scanning electron microscopy

The morphological characteristics of microscopic pores in transitional shales can be clearly observed through SEM. According to Loucks et al. (2012), microscopic pores can be classified as interparticle (interP) mineral pores, intraparticle (intraP) mineral pores, and intraP OM pores. InterP pores can be observed among different minerals, organic matter, and grains. IntraP pores are found within particles, such as interbedded pores of clay minerals. Both intraP and OM pores can be found within organic matter. Different types of pores have different morphological characteristics, and they can be distinguished by their brightness in SEM images. Metallic minerals (mainly pyrite) have the highest brightness; clay minerals and some clastic minerals, such as quartz or feldspar, have the second highest brightness; organic matter have the lowest brightness compared to all minerals. Because topography variation was highlighted by SEM imaging, pores are the darkest and can be easily identified (Jiao et al., 2012).

The SEM images showed that clay minerals and organic matter were in the main components of the transitional shale samples selected in this study (Fig. 8). Clay minerals mostly occurred as long gray strip combinations parallel to the bedding direction, with an inner lamellated microstructure, indicating that they had experienced strong compaction during burial (Fig. 8a and b) (Chen et al., 2016). The transitional shale of the Shanxi-Taiyuan Formation is in the high to over-mature stage of thermal evolution of organic matter, and has also experienced a long period of compaction. Most organic matter appeared as amorphous dark regions; in other words, the high over-maturity indicates the transitional shale samples undergoing a long period of OM thermal evolution and also high compaction (Fig. 8c, d, e). The main pores were interlayer pores of clay minerals, while SEM revealed poorly developed OM pores. In addition, a certain number of micro-fractures were also observed in the transitional shale samples (Fig. 8f).

5.2. Effect of sample damage on pore structure

Although the pore structure of shale has strong heterogeneity, for a millimeter-sized shale particle, the distribution of micropores, mesopores, and macropores can be considered uniform. An important prerequisite for the evaluation of shale powder samples by N_2 adsorption is that the crushing process exposes closed pores but does not create new pores. On this premise, regardless of how the sample particle size changes, the change rate of microporous pore volume (MiPV) and mesoporous volume (MePV) should be maintained at a constant value. The change in the SSA of shale also remains constant. Therefore, if the above assumption is true, the following equation is given:

$$MiPV_1 = a*MiPV_2 = a*MiPV_3 = \ldots = a*MiPV_n \quad (1)$$

$$MePV_1 = b*MePV_2 = b*MePV_3 = \ldots = b*MePV_n \quad (2)$$

$$SSA_1 = c*SSA_2 = c*SSA_3 = \ldots = c*SSA_n \quad (3)$$

where $MiPV_1$, $MiPV_2$ … $MiPV_n$ are the microporous pore volumes of shale samples when the particle size decreases sequentially, $MePV_1$, $MePV_2$ … $MePV_n$ are the mesoporous pore volumes of shale samples when the particle size decreases sequentially, SSA_1, SSA_2 …

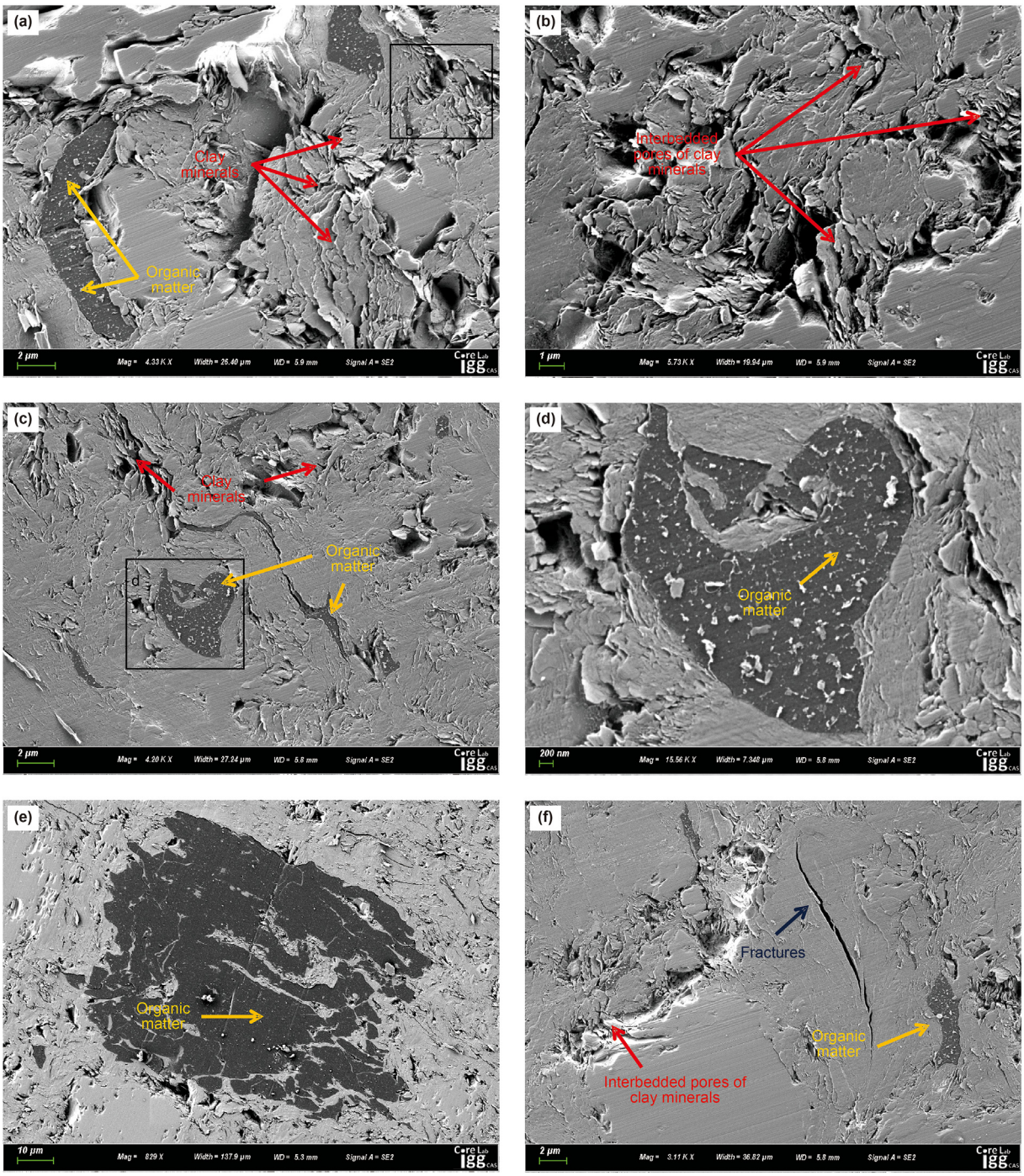

Fig. 8. SEM images of different pore types in the Shanxi and Taiyuan transitional shales. (a) The organic matter and clay minerals developed in the samples; (b) Clay minerals with typical layered structure and a large number of microscopic pores developed; (c) The organic matter in dark regions; (d) Magnified organic matter in zone C; (e) Fewer organic pores are visible; (f) Micro-fractures

SSA_n are the SSA of the shale sample when the particle size decreases successively, and *a, b,* and *c* are the coefficients.

However, in the actual use of gas adsorption methods to evaluate the microstructure of tight reservoirs, the manual preparation process of sample particles has a certain impact on the pore structure (Slatt and O'Brien, 2011; Lee, 2012; Boudriche et al., 2014; Pommer and Milliken, 2015). The analysis of the experimental data in the previous section revealed that the conventional manual sample preparation process damaged the pore structure of shale to a certain extent, resulting in the development of new pores or micro-fractures. Such a structural damage significantly affects the experimental results of the nitrogen adsorption experiment for evaluating the pore structure of shale.

5.2.1. Specific surface area

The SSA is often closely related to the micropore content of the sample. Under the same circumstances, assuming that the total PV of the sample is certain, the smaller the particle size, the larger the surface area (Han et al., 2016). With an increase in the crushing mesh, the particle size decreased continuously, while the SSA

values of these samples showed little changes (Fig. 4a) (Mastalerz et al., 2017). In the process of crushing the samples from 20 to 200 mesh, the particle size decreased to 75 μm, which is insufficient to destroy micropores with a pore size of less than 2 nm in the nanoscale pore structure. Therefore, the change in micropores with the number of experimental crushing meshes is not significant, and the sample preparation process has little influence on the change in SSA (Wei et al., 2014; Chen et al., 2015).

5.2.2. Pore volume

In the discussion of the experimental data, the PV widely varied during the crushing of samples with mesh number increasing from 20 to 80 and 200 (Fig. 4b), and the increase range of the PV of different pore types also followed different rules (Fig. 5a–c). As the samples were continuously crushed from 20 mesh to 200 mesh, the effect of crushing on the level of micropores with pore sizes less than 2 nm can be ignored; that is, the SSA and PV of micropores measured in the nitrogen adsorption experiment showed little change with sample particle size. Therefore, the significant increase of PV value is mainly due to the sample preparation damage, resulting in secondary pores or fractures. These newly produced pores are mainly mesopores and macropores. With the increase of crushing meshes in the sample preparation process, the change rules of the PV value can be classified into three types (Fig. 9):

a. **With increasing crushing mesh, the growth rate of the PV increases.** In this case, as the particle size decreased, the PV increased rapidly. This indicates that new connected pores or fractures are constantly produced during the sample preparation process. The number of mesopores and macropores continued to increase, increasing the PV of the shale samples. At this time, the pore structure was not completely destroyed, and the continuous generation of connected pores contributed to the PV.
b. **PV increases uniformly with the mesh number.** In this case, as the particle size decreased, the PV maintained a trend of linear growth. When the sample was crushed to 200 mesh, the pore structure was uniform at the microscopic pore level and was not destroyed during the sample preparation process. The PV exhibited a linear growth, which reflects that the pore structure of the shale samples is relatively uniform.
c. **With increasing crushing mesh, the growth rate of the PV decreases.** In this case, as the particle size decreases, the trend of PV growth gradually slows down, indicating that the PV of the shale samples did not increase substantially during the process of crushing to 200 mesh. However, there was a certain maximum growth rate. When it is less than the maximum growth rate of the PV value, new connected pores (mesopores, macropores, or micro-fractures) are constantly generated, resulting in a significant increase in the PV. When it is greater than the maximum growth rate of the PV value, there are fewer or no new connected pores in the sample, and micro-fractures cannot be connected with closed pores. At this time, the pore structure is seriously damaged, and the PV of the sample changes slowly or even stops changing after reaching a certain critical value.

According to the experimental data, the variation law of the pore system conforms to the third case (Figs. 4b and 5). With increases in crushing meshes, new pores were generated in the pore-fracture system of the shale samples. These pores can be connected by the increasing micro-fractures, which provide more adsorption space for liquid nitrogen, and further increase the PV of the sample. At the same time, as the degree of damage increases, the supporting structure of the pores may be damaged when a critical value of the supporting pore lattice is reached in the sample preparation process, resulting in the formation of micropores during the damage process and destruction of pores. Meanwhile, the increase in PV decreases or even stops increasing. The changes in the pore-fracture system induced by damage during sample preparation have a certain error effect on the qualitative and quantitative research of pore structure in shale samples, and this error cannot be ignored.

5.2.3. Ratio of specific surface area to pore volume (SSA/PV)

The solid medium of shale is heterogeneous and complex in structure, mixed with organic matter and mineral components. The proportions of pores with different particle sizes, such as micropores, mesopores, and macropores, are also different. Generally, the SSA, PV, PSD, and other single parameters are used to describe the structural characteristics of microscopic pore systems. However, during the sample preparation process, the changes in the mesh number may damage the internal pore structure owing to the different components and structures of the solid matrix. Considering the possibility of nanoscale pore structure changes during manual sample preparation and the limitation of a single parameter, this study proposed a comprehensive description of the changes in the micropore structure in tight shale by calculating SSA/PV.

In the shale samples studied, the relationship between PV and SSA with the increasing crushed meshes calculated for each sample is shown in Fig. 10a. A weak correlation was observed between PV and SSA. Further statistics of the change in the SSA/PV ratio are shown in Fig. 10b. The SSA/PV decreased with increasing mesh number, and when the crushing mesh reached the maximum PV growth rate, the decreasing amplitude of SSA/PV gradually slowed down. The change in SSA/PV with the number of crushing meshes was well consistent with the change in PV with increasing crushing mesh.

Compared with a single parameter that characterizes the pore structure (such as SSA, PV, etc.), SSA/PV can more comprehensively reflect the changes in the microscopic pore structure of shale

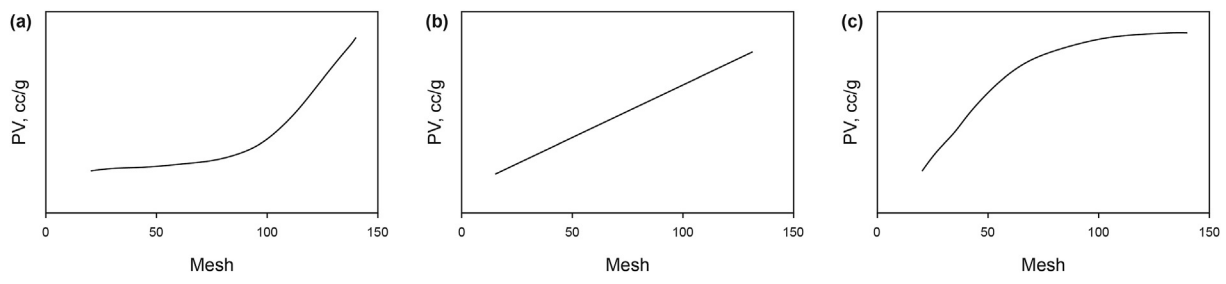

Fig. 9. The changes of pore volume with crushing mesh.

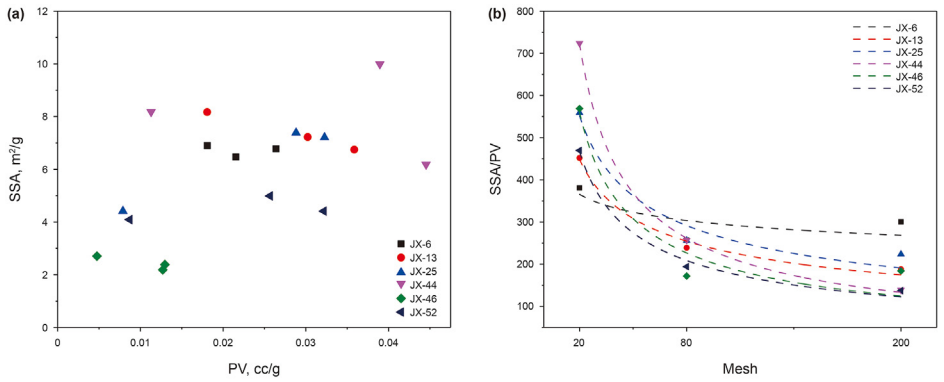

Fig. 10. The relation between PV and SSA under different meshes (a), and the change of SSA/PV under different meshes (b).

samples and the degree of damage of various pores in the sample preparation process of gas adsorption experiments. Similar to the change in PV in the sample preparation process, the possible changes in SSA/PV can be divided into the following three categories:

(i) SSA/PV increases with increasing degree of damage.

As the degree of damage has little effect on the micropores, the overall change in the SSA is small. PV increases with increasing crushing mesh, and SSA/PV increases. This shows that ΔSSA increases significantly, and the increment of micropores is larger than that of mesopores. In other words, with increasing mesh number during sample preparation, the PV and quantity ratio of micropores in the connected pores play a leading role in changing the pore structure.

(ii) SSA/PV remains unchanged or changes at a small amplitude.

The shale sample was relatively homogeneous, and the SSA and PV changed to the same degree; in other words, the changes in micropores and mesopores were consistent. This indicates that the influence of the sample preparation process on the quantity and PV of various shale pores was consistent.

(iii) SSA/PV decreases with increasing damage degree.

As the degree of damage has little effect on the micropores, the overall change in SSA is small. PV increases with increasing crushing mesh, but SSA/PV decreases. This shows that ΔPV has a larger increase, and the increment of mesopores and macropores is larger than that of micropores. In other words, as the crushing meshes increased during the sample preparation process, the particle size of the samples continued to decrease, and additional interconnected pores were possibly generated during the crushing process (the mesopores became connected to form macropores, the number of macropores increased, or new shrinkage fractures developed due to stress). PV increased significantly, and the sample preparation process damaged the pore structure to a certain extent, leading to errors in the measured experimental data.

Comparing the change rates of SSA/PV values among different samples, the damage induced by sample preparation leads to certain errors in the data of the traditional pore structure test, which affects oil and gas exploration results. Therefore, the relevant characterization data must be corrected. The results also show that it is feasible to use the change in SSA/PV with mesh number as a qualitative method for identifying the change in microscopic pore structure during sample preparation and for evaluating the accuracy of the pore structure test characterization data of samples with nanoscale pore structure in tight reservoirs.

5.3. Main controlling factors of transitional shale pore structure variation

The characterization of the pore structure is an important basis for evaluating the performance of tight reservoirs (Loucks et al., 2012). The thermal evolution of organic matter in the transitional shale from the Shanxi and Taiyuan Formations is generally mature, and SEM revealed relatively poor development of OM pores; the pore structure is dominated by clay mineral pores (Peng et al., 2017). According to the results of the above low-temperature N_2 adsorption experiment, pore structure parameters such as SSA, PV, and adsorption capacity of limestone sample JX-46 showed little change with increasing crushing mesh number. The pore structure parameters of the other five samples varied with decreases in particle size. To accurately study the microscopic pore structure of transitional shale, it is necessary to distinguish the main factors affecting the development of various pores in the pore-fracture system.

Coal is a porous heterogeneous mixture composed of organic macerals and a small amount of inorganic minerals. The pores are dominated by OM pores, and coal-matrix pores are mainly affected by TOC (Xu and Zhu, 2020). Tight sandstone reservoirs are mainly composed of heterogeneous mixtures of various porous minerals. The pore types are mainly inorganic pores, and pore development is controlled by the content of mineral components in the reservoir (Sun et al., 2020). The development of microscopic pores in marine shale is influenced by both TOC and mineral component content. Therefore, in this study, we applied factors affecting the pore development of marine shale for comparing the pore characteristics of the transitional shale samples, and focused on discussing the development characteristics of various pores in marine continental transitional shale.

5.3.1. Relationship between TOC and pore structure variation

Organic matter is the material basis for hydrocarbon formation in shale. Its internal structure is complex, and OM pores have a strong adsorption capacity. The OM content is of great significance for the generation and storage of gas in tight reservoirs. Previous studies have shown that with increasing OM content, the surface area of mud shale increases and the amount of adsorbed gas also increases gradually (Chalmers and Bustin, 2008; Zhang et al., 2012). Pores in marine continental transitional shale are mainly developed in clay minerals and organic matter. The TOC content of the Shanxi and Taiyuan Formation shale samples was between 0.7% and 2%, with significant differences among these samples. The results of the

correlation analysis between TOC content and various types of pores in the marine and transitional shale samples are shown in Fig. 11 (Chen et al., 2015). Data of changes in marine shale samples were obtained from the New Albany Shale (NAS: Mastalerz et al., 2017) (Fig. 11a–c). Simple linear regression analysis showed that the correlation between TOC content and pore structure parameters (SSA, PV) showed little change with increasing degree of damage in transitional shale samples, and the linear correlation coefficient R^2 was between 0.003 and 0.6. TOC content showed good correlation with the development of pores in marine shale samples.

According to the experimental data, the development of various pores in transitional shale exhibited a weak correlation with TOC, compared with marine shale. A certain correlation was observed between micropores and TOC, whereas mesopores were generally not correlated with TOC. The increasing degree of damage had little influence on the correlation between microscopic pores and TOC. This further indicates that TOC content has a certain influence on the development of micropores in transitional shale from the Shanxi and Taiyuan Formations, although the influence is weak. Damage from sample preparation did not destroy the pore structure of the micropores, but only increased the number and volume of micropores to a certain extent. Micropores and small mesopores largely contributed to SSA.

5.3.2. Relationship between mineral composition and pore structure variation

The content and composition of minerals in shale can reflect the sedimentary and diagenetic environment and play a certain role in controlling pore development as well as the generation and storage of shale gas. In general, the higher the content of brittle minerals in shale, such as quartz, feldspar, and calcite, the more likely the formation of fractures under the influence of compression, thus improving the extraction rate of shale gas. The higher the clay mineral content, the more complex the pore structure of shale, which is helpful for increasing the surface area and PV. A typical characteristic of marine continental transitional shale is the development of a large number of clay mineral pores, which can significantly increase the adsorption capacity (Loucks et al., 2012; Cai et al., 2013; Han et al., 2013).

The results of the correlation analysis between clay mineral content and various types of pores in the marine and transitional shale samples are shown in Fig. 12. The image shows that the clay mineral content significantly affects the pore structure parameters (SSA, PV) of micropores and mesopores in transitional shale, while the influence is very small for marine shale (Fig. 12a–c). The linear correlation coefficient (R^2) of transitional shale samples is generally distributed between 0.7 and 0.9 (Fig. 12d–f), which indicates that the pore types developed in clay minerals are mainly micropores and small mesopores. In addition, increases in the degree of damage have little effect on the correlation between micropores and clay mineral content, but they significantly affect the correlation between mesopores and clay mineral content. Furthermore, damage from sample preparation processes can destroy the internal structure of clay minerals to a certain extent. The pore structure of the micropores was not significantly affected, and the damage mainly destroyed the pore structure of larger pores. Increases in the number and volume of mesopores and larger pores led to changes in pore structure parameters.

The experimental data showed that the clay mineral content is the most important factor affecting the pore development of the Shanxi and Taiyuan Formation transitional shale samples. The clay minerals in the samples were mainly illite, with a relatively small amount of illite-smectite mixed clay (I/S). To further explore the specific clay mineral playing a major role in the development of various types of pores, the contents of illite and I/S, which account for the largest proportion of clay minerals, were analyzed, and their effects on pore structure parameters with increasing degree of damage were investigated (Figs. 13 and 14).

The regression analysis showed that with increasing degree of damage, the contents of I/S and illite are related to the structural

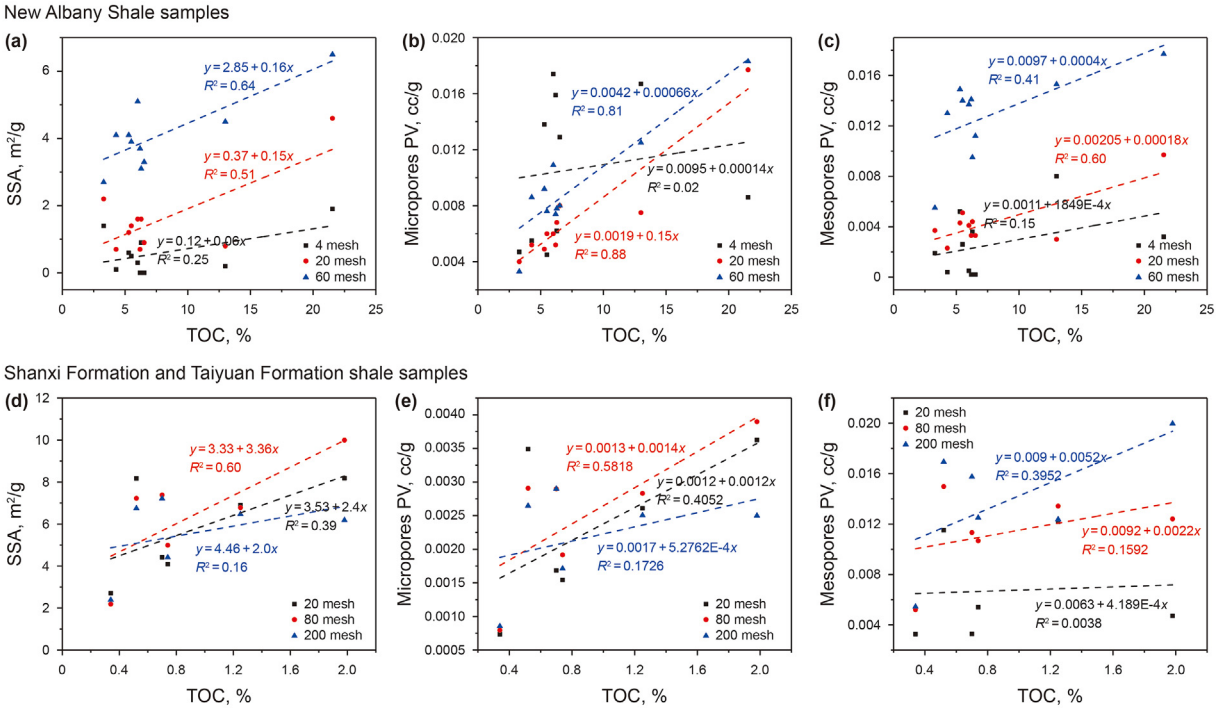

Fig. 11. The correlation between TOC content and various pores (Among them, a, b, c are derived from the NAS marine shale samples, data from Chen et al., 2015; d, e, f are derived from the Shanxi Formation and Taiyuan Formation transitional shale samples.)

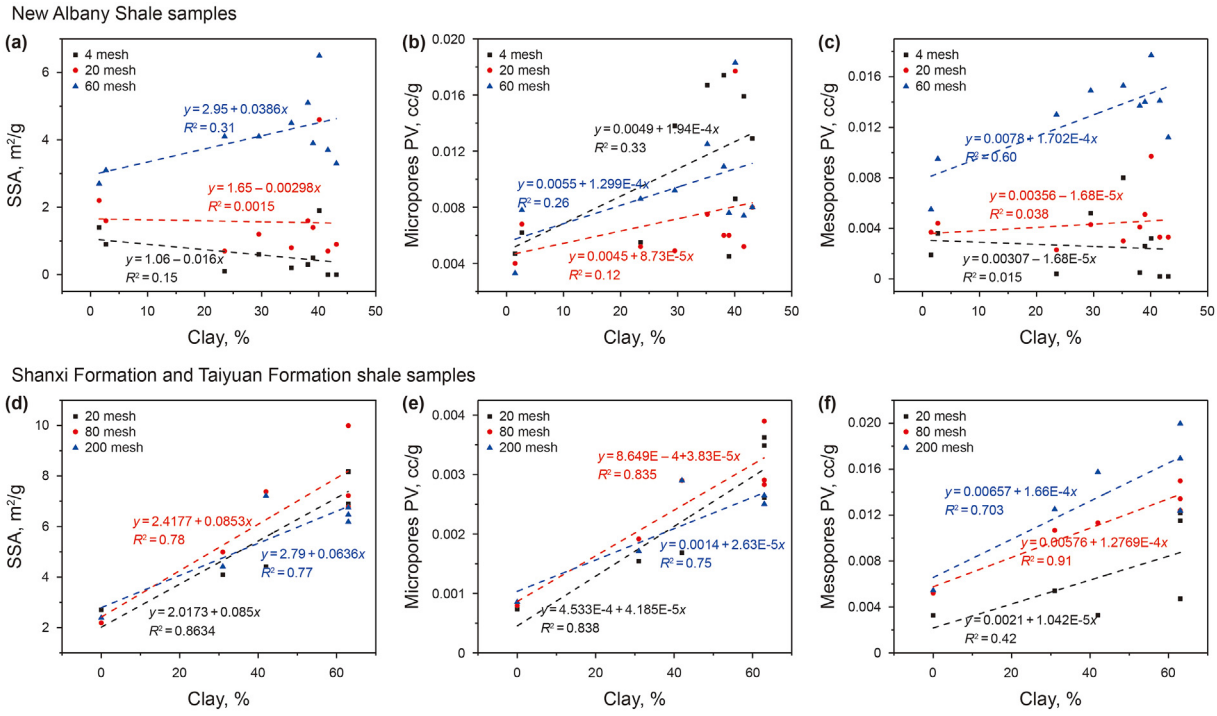

Fig. 12. The correlation between clay mineral content and various pores (Among them, a, b, c are derived from the NAS marine shale samples, data from Chen et al., 2015; d, e, f are derived from the Shanxi Formation and Taiyuan Formation transitional shale samples.)

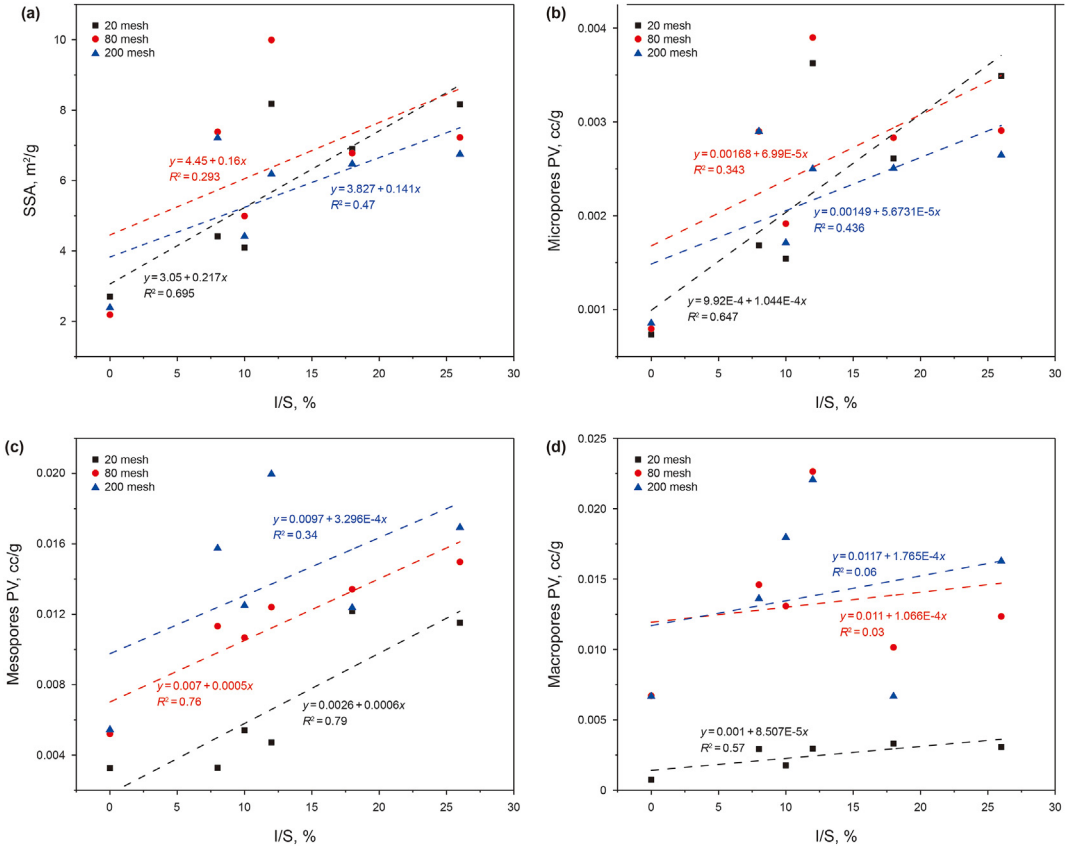

Fig. 13. The correlation between I/S content and various pores of transitional shale samples in the study area.

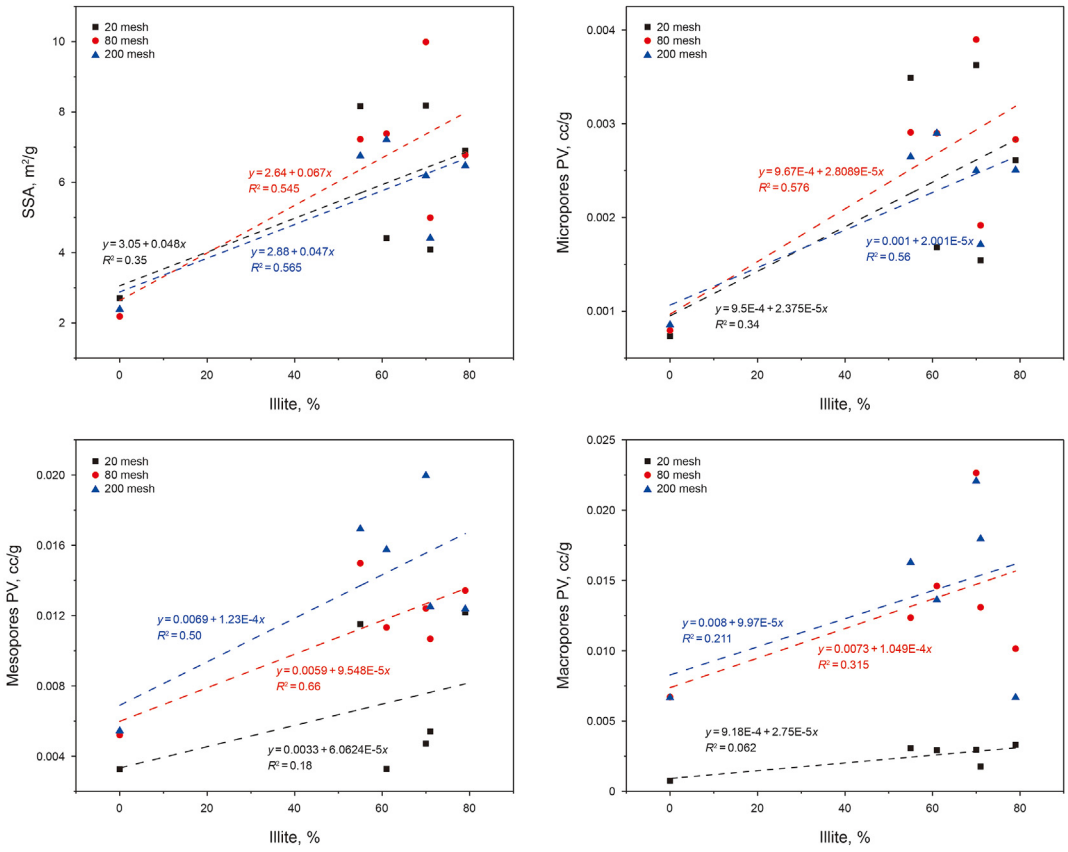

Fig. 14. The correlation between illite content and various pores of transitional shale samples in the study area.

parameters of micropores and mesopores (SSA, PV), and the linear correlation coefficient R^2 ranged from 0.2 to 0.8. However, no correlation was observed between the contents of illite and I/S, and macropores. With crushing at 20 mesh, the micropores and mesopores were mainly affected by the I/S content. When the crushing mesh was increased to 80, the correlation between micropores and I/S weakened, while that between micropores and illite strengthened. The correlation between mesopores and illite was significantly enhanced, indicating that mesopores were mainly influenced by the contents of illite and I/S. The correlation coefficient reached the maximum among all influencing factors. When the crushing mesh was increased to 200, the correlation between micropores and the content of illite and I/S became weak, similar to that for mesopores. This finding suggests that clay minerals are the main factor affecting the development of micropores and mesopores, and macropores are not controlled by a single component but influenced by the combined action of multiple factors. To a certain extent, increases in the degree of damage leads to the generation of new connected pores (macropores are broken into mesopores, or the originally existing closed pores are connected by micro-fractures), and PV increases rapidly. However, if the crushing mesh is too large, the internal pores of clay minerals (mainly I/S) are destroyed, weakening the correlation between micropores, mesopores, and clay minerals (illite, I/S).

Based on the above findings, TOC and clay mineral content affect the development of micropores in shale. For the marine continental transitional shale of the Shanxi and Taiyuan Formations, clay minerals with micropores and small mesopores play a leading role in pore development, and TOC content also affects pore development to a certain extent. This is different from the main controlling factors of pore development in marine shale. Most of the organic matter in sedimentary rocks associate with clay minerals in the form of complexes (Cai et al. 2007, 2013; Fan et al., 2011). Transitional shale in China is characterized by rich organic matter and highly mature evolution. As this shale has experienced overcompaction and is at an over-mature stage of thermal evolution, the amounts of interparticle pores and intraparticle pores are small. The internal structure of clay minerals is relatively complex, and clay minerals contain a large number of OM particles. The symbiotic relationship between clay minerals and organic matter plays an important role in promoting the development of micropore systems in tight shale reservoirs and also affects the gas content of the shale reservoir. Therefore, there is a complex interaction between organic matter and clay minerals, and the symbiotic relationship between them has a microcosmic influence on the pore structure of shale reservoirs at the nanometer scale. Nevertheless, the macroscopic impact of this relationship on shale gas content requires further study.

5.3.2.1. Limitations. The experimental methods and samples in present study have some limitations. Nitrogen adsorption experiments have been widely accepted for decades as the standard method for micropore and mesoporous pore size analysis. However, due to the structural characteristics of nitrogen molecules, it is difficult to quantify micropores, especially ultra-micropores. In this research, in the process of calculating the pore volume of micropores and mesopores, the molecular dynamic method NLDFT calculation model is used to analyze the pore volume, so as to further reduce the influence of the limitations of the experiment on the data. In addition, only 6 samples were studied when the factors affecting the change of pore structure were discussed from different perspectives. The number of samples is small, but the

overall rule is clear, which can reflect the change of pore structure under the control of different factors. For similar studies, more samples may be needed for further discussion.

6. Conclusions

In this study, experiments combining low-temperature N_2 adsorption with organic petrography and mineralogical analysis (TOC, R_o, XRD, and SEM) were performed to analyze the influence of structural damage on microscopic pore development in the transitional shale samples of the Shanxi and Taiyuan Formations. Changes in pore structure parameters with different degrees of damage and the relationship between pore types and the main controlling factors were determined. The main conclusions are as follows:

(1) In the analysis of the microscopic pore structure characteristics of transitional shales of the Shanxi and Taiyuan Formations based on the low-temperature nitrogen adsorption experiment, structural damage induced by sample preparation processes led to various changes in pore structure parameters (such as SSA, PV, PSD, etc.), which can lead to certain errors in the qualitative and quantitative evaluation of the microscopic pore system of tight reservoirs.

(2) With increasing degrees of structural damage, SSA changed within relatively tight bounds, while PV varied significantly. A certain critical value of growth rate (maximum) was observed in the process of increasing the crushing mesh number from 20 to 200. When the mesh was increased from 20 to the critical value (when the increase rate of PV is at the maximum), PV increased sharply. When the crushing mesh was increased from the critical value to 200, PV increased slowly or no longer increased.

(3) Under the actual formation conditions, the solid medium of shale is heterogeneous, and sample preparation processes change the internal pore structure. Compared to a single pore characterization parameter, the variation of SSA/PV could better reflect the possible change of various pores in the shale micropore system with increasing degrees of damage.

(4) The contents of TOC and clay minerals are the main factors controlling changes in the pore structure of the transitional facie shale of the Shanxi and Taiyuan Formations. Compared to the marine shales, the pore development of the transitional shale is dominated by clay mineral pores, and the clay mineral content plays a leading role in the microscopic pore structure of shale. In the study area, the most common clay minerals are illite and illite-smectite mixed clay, and they are both well correlated with changes in the structure of micropores and mesopores with increasing degrees of damage. The content of organic matter (TOC content) can also affect the development of microscopic pores, but it is not the main factor. TOC content and micropores exhibited a good correlation.

Acknowledgements

We gratefully acknowledge the financial support by the National Natural Science Foundation of China (Grant No. 41927801).

References

Ambrose, R.J., Hartman, R.C., Diaz-Campos, M., et al., 2012. Shale gas-in-place calculations Part I: new pore-scale considerations. Society of Petroleum Engineers 17 (1), 219–229. https://doi.org/10.2118/131772-PA.

Artur, P.Terzyk, Piotr, A.Gauden, Piotr, Kowalczyk, 2002. What kind of pore size distribution is assumed in the Dubinin–Astakhov adsorption isotherm equation? Carbon 40 (15), 2879–2886. https://doi.org/10.1016/S0008-6223(02)00219-1.

Bertard, C., Bruyet, B., Gunther, J., 1970. Determination of desorbable gas concentration of coal(direct method). International Journal of Rock Mechanics and Mining ences & Geomechanics Abstracts 7 (1), 43–65. https://doi.org/10.1016/0148-9062(70)90027-6.

Boudriche, L., Chamayou, A., Calvet, R., et al., 2014. Influence of different dry milling processes on the properties of an attapulgite clay, contribution of inverse gas chromatography. Powder Technol. 254, 352–363. https://doi.org/10.1016/j.powtec.2014.01.041.

Busch, A., Gensterblum, Y., Krooss, B.M., et al., 2004. Methane and carbon dioxide adsorption–diffusion experiments on coal: upscaling and modeling. Int. J. Coal Geol. 60 (2–4), 151–168. https://doi.org/10.1016/j.coal.2004.05.002.

Cai, J.G., Bao, Y.J., Yang, S.Y., et al., 2007. The occurrence form and enrichment mechanism of organic matter in argillaceous sediments and mudstones. Science in China(Series D). 37, 234–243. https://doi.org/10.3321/j.issn:1006-9267.2007.02.011 (in Chinese).

Cai, Z.R., Xia, B., Wan, Z.F., 2013. Characteristics of late tectonic activity and its influence on Paleozoic Shale gas preservation in Wuhu area of Lower Yangtze River. J. Coal Sci. Eng. (5), 890–895. CNKI:SUN:MTXB.0.2013-05-032 (in Chinese).

Chalmers, G.R.L., Bustin, R.M., 2008. Lower cretaceous gas shales in northeastern british columbia, part i: geological controls on methane sorption capacity. Bull. Can. Petrol. Geol. 56 (1), 1–21. https://doi.org/10.2113/gscpgbull.56.1.1.

Chen, Q., Zhang, J., Tang, X., et al., 2016. Relationship between pore type and pore size of marine shale: an example from the Sinian-Cambrian formation, upper Yangtze region, South China. Int. J. Coal Geol. 158 (15), 13–28. https://doi.org/10.1016/j.coal.2016.03.001.

Chen, Y., Wei, L., Mastalerz, M., et al., 2015a. The effect of analytical particle size on gas adsorption porosimetry of shale. Int. J. Coal Geol. 138 (15), 103–112. https://doi.org/10.1016/j.coal.2014.12.012.

Chen, Y., Zou, C., Mastalerz, M., et al., 2015b. Applications of micro-fourier transform infrared spectroscopy (FTIR) in the geological sciences–A review. Int. J. Mol. Sci. 16 (12), 30223–30250. https://doi.org/10.3390/ijms161226227.

Dang, W., Zhang, J.C., Tang, X., et al., 2018. Investigation of gas content of organic-rich shale: a case study from Lower Permian shale in southern North China Basin, central China. Geoscience Frontiers 9 (2), 559–575. https://doi.org/10.1016/j.gsf.2017.05.009.

Desbois, G., Urai, J.L., Kukla, P.A., et al., 2011. High-resolution 3D fabric and porosity model in a tight gas sandstone reservoir:A new approach to investigate microstructures from mm- to nm-scale combining argon beam cross-sectioning and SEM imaging. J. Petrol. Sci. Eng. 78 (2), 243–257. https://doi.org/10.1016/j.petrol.2011.06.004.

Fan, F., Cai, J.G., Xu, J.L., et al., 2011. The original occurrence state of different organic macerals in argillaceous hydrocarbon source rock. J. Tongji Univ. Nat. Sci. 39 (3), 434–439. https://doi.org/10.3969/j.issn.0253-374x.2011.03.023 (in Chinese).

Gao, H., Li, H.A., 2016. Pore structure characterization, permeability evaluation and enhanced gas recovery techniques of tight gas sandstones. J. Nat. Gas Sci. Eng. 28, 536–547. https://doi.org/10.1016/j.jngse.2015.12.018.

Gu, X., Cole, D.R., Rother, G., et al., 2015. Pores in marcellus shale: a neutron scattering and FIB-SEM study. Energy Fuels 29 (3), 1295–1308. https://doi.org/10.1021/acs.energyfuels.5b00033.

Han, H., Cao, Y., Chen, S.J., et al., 2016. Influence of particle size on gas-adsorption experiments of shales: an example from a Longmaxi Shale sample from the Sichuan Basin, China. Fuel 186 (15), 750–757. https://doi.org/10.1016/j.fuel.2016.09.018.

Han, S.B., Zhang, J.C., Xing, Y.W., et al., 2013. The shale gas accumulation conditions and resource potential of Lower-Silurian Longmaxi Formation in southeastern Chongqing. J. Coal Sci. Eng. 38 (S1), 168–173. CNKI:SUN:MTXB.0.2013-S1-029 (in Chinese).

Jaroniec, M., 1983. Physical adsorption on heterogeneous solids. Adv. Colloid Interface Sci. 18 (3–4), 149–225. https://doi.org/10.1016/0001-8686(83)87002-X.

Jiang, N., 2016. Seismic exploration technology for shale gas in the Southern North China Basin. Petroleum Geology and Engineering 30 (2), 42–44. https://doi.org/10.3969/j.issn.1673-8217.2016.02.012 (in Chinese).

Jiao, S.J., Han, H., Weng, Q.P., et al., 2012. Scanning electron microscope analysis of porosity in shale. J. Chin. Electron Microsc. 31, 432–436. https://doi.org/10.3969/j.1000-6281.2012.05.011 (in Chinese).

Kuila, U., Prasad, M., 2013. Specific surface area and pore-size distribution in clays and shales. Geophysical Prospecting. 61(2-Rock Physics for Reservoir Exploration, Characterisation and Monitoring) 341–362. https://doi.org/10.1111/1365-2478.12028.

Landers, J., Gor, G.Y., Neimark, A.V., 2013. Density functional theory methods for characterization of porous materials. Colloid. Surface. Physicochem. Eng. Aspect. 437, 3–32. https://doi.org/10.1016/j.colsurfa.2013.01.007.

Lee, J., 2012. Grinding effects on the change of particle properties in cupric sulfide, CuS. Adv. Powder Technol. 23 (6), 731–735. https://doi.org/10.1016/j.apt.2011.09.004.

Li, C.M., Xue, H.T., Wang, M., et al., 2019. Influence of degassing temperature and sample size on the results of low-temperature nitrogen adsorption experiment on tight sandstone. Bull. China Soc. Mineral Petrol. Geochem. (2), 308–316. https://doi.org/10.19658/j.issn.1007-2802.2019.38.004 (in Chinese).

Li, Y., Wang, Z., Pan, Z., et al., 2019. Pore structure and its fractal dimensions of transitional shale: a cross-section from east margin of the Ordos Basin, China.

Fuel 241, 417–431. https://doi.org/10.1016/j.fuel.2018.12.066.
Loucks, R.G., Reed, R.M., Ruppel, S.C., et al., 2012. Spectrum of pore types and networks in mudrocks and a descriptive classification for matrix-related mudrock pores. AAPG (Am. Assoc. Pet. Geol.) Bull. 96 (6), 1071–1098. https://doi.org/10.1306/08171111061.
Mastalerz, M., Hampton, L., Drobniak, A., et al., 2017. Significance of analytical particle size in low-pressure N_2 and CO_2 adsorption of coal and shale. Int. J. Coal Geol. 178, 122–131. https://doi.org/10.1016/j.coal.2017.05.003.
Milner, M., Mclin, R., Petriello, J., 2010. Imaging Texture and Porosity in Mudstones and Shales: Comparison of Secondary and Ion-Milled Backscatter SEM Methods. Society of Petroleum Engineers. https://doi.org/10.2118/138975-MS.
Nandi, S.P., Walker Jr., P.L., 1975. Activated diffusion of methane from coals at elevated pressures. Fuel 54 (2), 81–86. https://doi.org/10.1016/0016-2361(75)90061-7.
Peng, C., Pan, J., Wan, X., 2017. Effects of clay minerals on pore structure and methane adsorption property of coal measure mud shale in Yuzhou Coalfield. China Coal 43, 46–52. https://doi.org/10.3969/j.issn.1006-530X.2017.06.011 (in Chinese).
Pommer, M., Milliken, K., 2015. Pore types and pore-size distributions across thermal maturity, Eagle Ford Formation, southern Texas. AAPG (Am. Assoc. Pet. Geol.) Bull. 99 (9), 1713–1744. https://doi.org/10.1306/03051514151.
Rietveld, W.J., MacKay, D.M., 1969. Evoked responses to acceleration and to tachistoscopic presentation of patterned visual stimuli. Electroencephalogr. Clin. Neurophysiol. 26 (5), 537. https://doi.org/10.2165/00128413-200615210-00030.
Ross, D.J.K., Bustin, R.M., 2009. The importance of shale composition and pore structure upon gas storage potential of shale gas reservoirs. Mar. Petrol. Geol. 26 (6), 916–927. https://doi.org/10.1016/j.marpetgeo.2008.06.004.
Slatt, R.M., O'Brien, N.R., 2011. Pore types in the Barnett and Woodford gas shales: contribution to understanding gas storage and migration pathways in fine-grained rocks. AAPG (Am. Assoc. Pet. Geol.) Bull. 95 (12), 2017–2030. https://doi.org/10.1306/03301110145.
Shi, M., Yu, B., Xue, Z., et al., 2015. Pore characteristics of organic-rich shales with high thermal maturity: a case study of the Longmaxi gas shale reservoirs from well Yuye-1 in southeastern Chongqing, China. J. Nat. Gas Sci. Eng. 26, 948–959. https://doi.org/10.1016/j.jngse.2015.07.042.
Strapoc, D., Mastalerz, M., Schimmelmann, A., et al., 2010. Geochemical constraints on the origin and volume of gas in the new Albany shale (Devonian-Mississippian), eastern Illinois basin. AAPG (Am. Assoc. Pet. Geol.) Bull. 94 (11), 1713–1740. https://doi.org/10.1306/06301009197.
Sun, T., Zhang, Z.Q., Shi, Y.M., et al., 2020. Characterization of nanoscale pore distribution of tight sandstone reservoirs based on nitrogen adsorption. Special Oil Gas Reservoirs 27 (2), 145–151. https://doi.org/10.3969/j.issn.1006-6535.2020.02.023 (in Chinese).
Tang, S., Zhan, J.C., Elsworth, D., et al., 2016. Lithofacies and pore characterization of the lower permian Shanxi and taiyuan shales in the Southern North China basin. J. Nat. Gas Sci. Eng. 36, 644–661. https://doi.org/10.1016/j.jngse.2016.11.013.
Thommes, M., Kaneko, K., Neimark, A.V., et al., 2015. Physisorption of gases, with special reference to the evaluation of surface area and pore size distribution (IUPAC Technical Report). Pure Appl. Chem. 87 (9–10), 1051–1069. https://doi.org/10.1515/pac-2014-1117.
Tian, H., Pan, L., Xiao, X., et al., 2013. A preliminary study on the pore characterization of Lower Silurian black shales in the Chuandong Thrust Fold Belt, southwestern China using low pressure N_2 adsorption and FE-SEM methods. Mar. Petrol. Geol. 48, 8–19. https://doi.org/10.1016/j.marpetgeo.2013.07.008.
Tong, S., Dong, Y., Zhang, Q., et al., 2017. Quantitative analysis of nanopore structural characteristics of lower paleozoic shale, chongqing (southwestern China): combining FIB-SEM and NMR cryoporometry. Energy Fuels 31 (12), 13317–13328. https://doi.org/10.1021/acs.energyfuels.7b02391.
Wang, G., Chang, X., Yin, W., et al., 2017. Impact of diagenesis on reservoir quality and heterogeneity of the Upper Triassic Chang 8 tight oil sandstones in the Zhenjing area, Ordos Basin, China. Mar. Petrol. Geol. 83, 84–96. https://doi.org/10.1016/j.marpetgeo.2017.03.008.
Wei, L., Mastalerz, M., Schimmelmann, A., et al., 2014. Influence of Soxhlet-extractable bitumen and oil on porosity in thermally maturing organic-rich shales. Int. J. Coal Geol. 132, 38–50. https://doi.org/10.1016/j.coal.2014.08.003.
Xiong, F., Jiang, Z., Li, P., et al., 2017. Pore structure of transitional shales in the Ordos Basin, NW China: effects of composition on gas storage capacity. Fuel 206, 504–515. https://doi.org/10.1016/j.fuel.2017.05.083.
Xu, Y.B., Zhu, Y.S., 2020. Pore structure characteristics of high rank coal and influence on coalbed methane desorption. Natural Gas Geoscience 31 (1), 84–92. https://doi.org/10.11764/j.issn.1672-1926.2019.10.006 (in Chinese).
Yang, C., Zhang, J., Tang, X., et al., 2017. Comparative study on micro-pore structure of marine, terrestrial, and transitional shales in key areas, China. Int. J. Coal Geol. 171, 76–92. https://doi.org/10.1016/j.coal.2016.12.001.
Yang, F., Ning, Z., Wang, Q., et al., 2016. Pore structure characteristics of lower Silurian shales in the southern Sichuan Basin, China: insights to pore development and gas storage mechanism. Int. J. Coal Geol. 156, 12–24. https://doi.org/10.1016/j.coal.2015.12.015.
Yang, Z.H., Martias, T., 2009. Progress in pore size analysis by gas adsorption: application of density function theory(DFT) and Monte Carlo method(MC). China Powder Industry 6, 36–42 (in Chinese). JournalArticle/5af5324cc095d718d8228222.
Zhang, D.Z., 2017. Using nitrogen adsorption experiment to analyze the microscopic pore structure characteristics of tight sandstone reservoirs:Taking the Shahezi Formation of Xujiaweizi Depression in Songliao Basin as an example. Natural Gas Geoscience 28 (6), 898–908. https://doi.org/10.11764/j.issn.1672-1926.2017.05.004 (in Chinese).
Zhang, L., Lu, S., Xiao, D., et al., 2017. Pore structure characteristics of tight sandstones in the northern Songliao Basin, China. Mar. Petrol. Geol. 88, 170–180. https://doi.org/10.1016/j.marpetgeo.2017.08.005.
Zhang, T., Ellis, G.S., Ruppel, S.C., et al., 2012. Effect of organic-matter type and thermal maturity on methane adsorption in shale-gas systems. Org. Geochem. 47, 120–131. https://doi.org/10.1016/j.orggeochem.2012.03.012.
Zou, C., Zhu, R., Liu, K., et al., 2012. Tight gas sandstone reservoirs in China: characteristics and recognition criteria. J. Petrol. Sci. Eng. 88-89, 82–91. https://doi.org/10.1016/j.petrol.2012.02.001.